Supplementary Information for:

Interplay between Connectivity and Passivating Agents in Perovskite Quantum Dot Networks

María Morán-Pedroso[#], David O. Tiede[#], Carlos Romero-Pérez, Mauricio E. Calvo, Juan F. Galisteo-López*, Hernán Míguez*.
Instituto de Ciencias de Materiales de Sevilla (Consejo Superior de Investigaciones Científicas-Universidad de Sevilla), C/Américo Vespucio, 49, Sevilla, 41092, Spain.

**E-mail: juan.galisteo@csic.es, h.miguez@csic.es*

#Equal contributors

S.1 Experimental

S.1.1 Sample fabrication

S.1.2 Absorption and photoluminescence measurements

S.1.3 Time-resolved photoluminescence measurements

S.2 Absolute PL spectra for different $FAPbBr_3@SiO_2$ samples under study

S.3 Irradiation/recovery PL curves for $FAPbBr_3@SiO_2$ samples in N_2 atmosphere

S.5 Spectral evolution of PL of $FAPbBr_3@SiO_2$ samples under CW irradiation

S.6 Normalized PL spectra for the 5% $FAPbBr_3@SiO_2$ sample

S.7 Activation/recovery PL curves for samples passivated with PMMA

S.8 Spectral evolution of PL under CW irradiation for passivate samples

S.9 Activation/recovery PL curves for samples exposed to an O_2 atmosphere

S.10 Activation/recovery PL curves for samples exposed to a humid air atmosphere

S.11 Lognormal fits of TRPL data for samples fabricated with 5% precursor and exposed to different passivating agents

S.1 Experimental

S.1.1 Sample fabrication

Materials*:* Methanol (MeOH, *VWR*, 98%), 30 nm SiO_2 nanoparticles (34% w/v in H_2O, LUDOX-TMA, Sigma-Aldrich), Dimethylsulfoxide (DMSO, *Merck*, anhydrous 99.8%), Lead (II) bromide ($PbBr_2$, TCI, 99,99%), Formamidinium bromide (FABr, GreatCell Solar Materials, 99,9%), Chlorobenzene (CB, *Merck*, 99.9%), Poly(methylmethacrylate) (PMMA, MW:400000-550000, Alfa Aesar, 99.9%) were used as received.

SiO_2 porous scaffold: a dilution in Methanol of 3%w/v of LUDOX-TMA 30nm SiO_2 nanoparticles suspension is deposited by dip-coating applying a withdrawal speed of 120 mm/min. This process is performed 15 times in total to obtain a scaffold with a thickness around 1.1 µm. A thermal annealing at 450ºC for 30 min is applied to remove any remaining organic component as well as for hardening the porous scaffold

Scaffold assisted synthesis of $FAPbBr_3$ QD: perovskite solutions are prepared dissolving FABr and $PbBr_2$ in a 1:1 molar ratio in DMSO and infiltrating it inside the porous scaffold via spin-coating at 5000 rpm for 60 s. A thermal treatment at 100ºC for 1 h provides solvent evaporation and $FAPbBr_3$ crystallites formation. QD loading inside the film can be adjusted varying solution concentration used in this process (see Table S1). This process is done inside a N_2-filled glovebox with <0.5ppm background humidity.

Average NC size and interparticle separation were estimated according to a previously published procedure. [1] Extracted values are listed in Table S1:

Precursor concentration C_{prec}	Fill fraction *ff*	Estimated <*r*>	# of QDs per m^3	d_{center}	d_{interp}
5 %	0.0141	4.5 nm	$3.7 \cdot 10^{22} m^{-3}$	37 nm	28 nm
10 %	0.0405	5.7 nm	$5.2 \cdot 10^{22} m^{-3}$	33 nm	22 nm
20 %	0.092	6.26 nm	$9.0 \cdot 10^{22} m^{-3}$	28 nm	15 nm

Table S1: fill fraction (extracted from Inductively coupled plasma mass spectrometry measurements), average NC radius, number of NCs per m^3, center-to-center and interparticle separation estimated as described in [1].

PMMA FAPbBr3 QD treatment: PMMA is dissolved in CB (10 mg/mL) at 50ºC for 1 hour under stirring. Once complete dissolution has been achieved and the solution has cooled down to room temperature,150 µL are added to FAPbBr3 QD films and spin coated at 5000 rpm for 60 seconds. This is followed by an annealing step of 90ºC for 60 minutes. The aforementioned procedure is conducted within an N2-filled glovebox.

Grazing-Incidence X-Ray Diffraction characterization: X-Ray diffractograms were obtained using an Empyrean diffractometer (Malvern Panalytical) configured in a Grazing Incidence mode, with Cu Kα radiation (λ = 1.54518 Å), over a range of 10-50º, with a 0.05º step size and a 4-second count time per step.

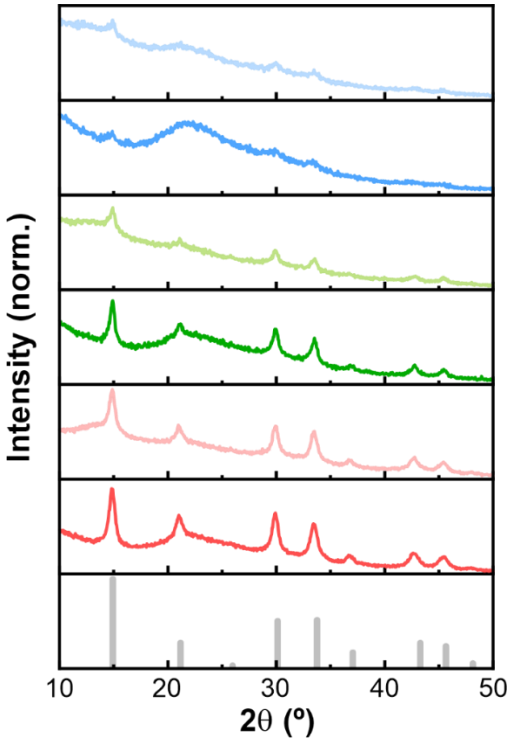

Figure S1. GIXRD characterization under atmospheric conditions of $FAPbBr_3$ QD films corresponding to 5 (blue), 10 (green) and 20% (red) precursor solution concentration. Neat samples correlate to darker curves while those treated with PMMA are represented in lighter colors. Reference cubic pattern (modeled) is inserted at the bottom as gray columns.

S.1.2 Absorption and photoluminescence measurements

Absorption was measured with a Cary 5000 spectrophotometer (UV–vis–NIR) equipped with a DRA-2500 (PMT/PbS) detector. Absorptances were estimated from the total transmittance and total reflectance measurements in the VIS range.

All emission measurements were carried out irradiating with a tunable pulsed laser (Fianium SuperK from NKT) operating at different repetition rates (RR) with a pulse length of 900ps and a spot size of 150 μm. For PL measurements a RR=40MHz and λ=450nm was used with an average power of 600μW. A long focal length (f=10cm) achromatic lens is used for both optical excitation and collection. The latter is performed with a fiber coupled spectrophotometer (Flame-T from Ocean Insight).

S.1.3 Time-resolved photoluminescence measurements

TRPL measurements were carried out using a Time Correlated Single Photon Counting card (SPC-130-EMN from Becker & Hickl). Optical excitation was performed with the above-mentioned pulsed laser with a RR in the 0.2-5 MHz range (depending on sample PL dynamics) and a spectral window λ=450-485nm. Spot size was the same as above. PL was collected with an avalanche photo diode (id100 from ID Quantique). For each sample, measurements were carried out for different average powers: 0.1, 0.3, 1, 3 and 10 μW.

S.1.4 Exposure to different environmental conditions

In order to ensure that the atmosphere surrounding the sample was completely replaced in the different measurements, the sample was placed in a home-built flow chamber with a sample space only slightly larger than the sample surface. A sufficiently large flow was employed so that the volume of the sample chamber was replaced several times per minute.

S.2 Absolute PL spectra for different $FAPbBr_3@SiO_2$ samples under study

PL measurements under identical conditions were measured for the different $FAPbBr_3@SiO_2$ samples under study in order to evidence the change in PLQY due to varying connectivity. Results are shown in **Figure S1**.

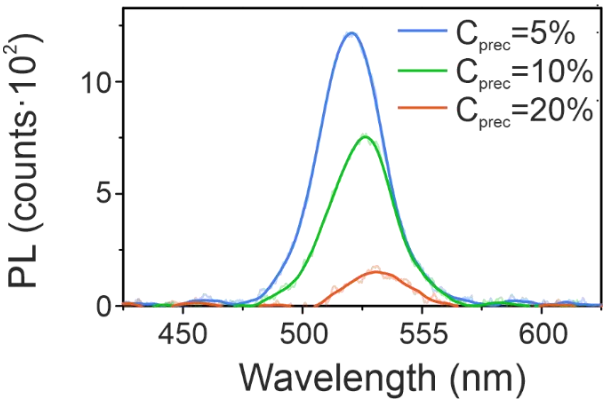

Figure S2: (a) Absolute PL spectra for $FAPbBr_3@SiO_2$ samples with different precursor load/average interparticle separation: 5%/28nm (blue), 10%/22nm (green) and 20%/15nm (red curve.)

S.3 Irradiation/recovery PL curves for $FAPbBr_3@SiO_2$ samples in N_2 atmosphere:

Figure S2 shows the time evolution of the PL of a 5% $FAPbBr_3@SiO_2$ sample when irradiated under CW light and subsequent recovery in the dark.

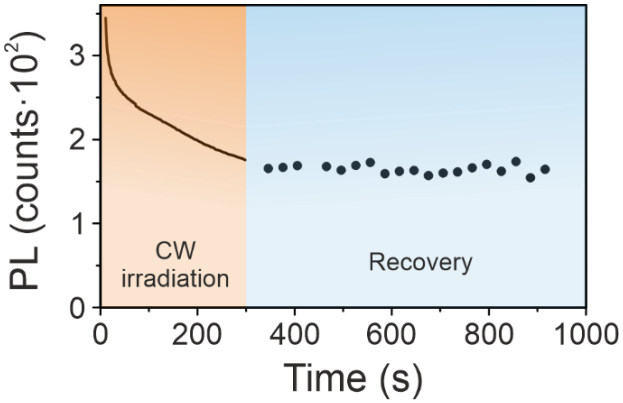

Figure S3: Time evolution of the PL maximum for a $FAPbBr_3@SiO_2$ sample with C_{prec}=5% in a N_2 atmosphere under CW irradiation (orange box) and under recovery in the dark (blue box).

S.4 Spectral evolution of PL of $FAPbBr_3@SiO_2$ samples under CW irradiation:

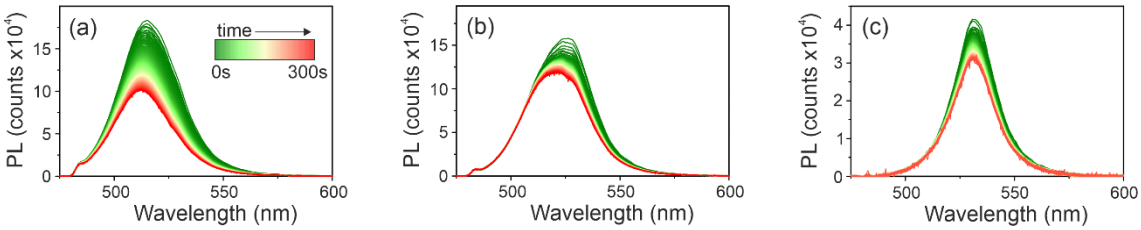

Figure S4: PL spectra collected at different times (same time span as in Figure 1 in the main text) under CW irradiation for $FAPbBr_3@SiO_2$ samples with different precursor load/interparticle separation: (a) 5%/28nm, (b) 10%/22nm and (c) 20%/15nm.

S.5 Normalized PL spectra for the 5% $FAPbBr_3@SiO_2$ sample:

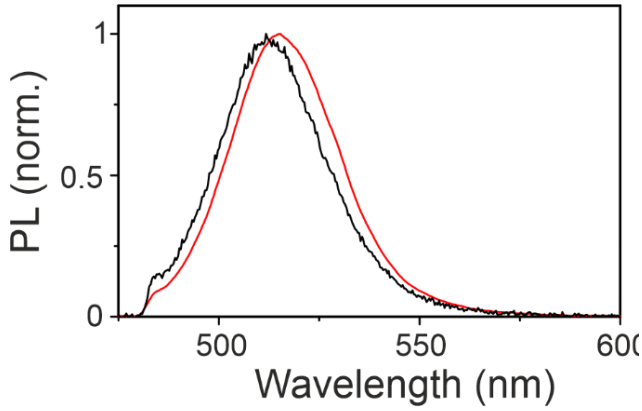

Figure S5: Normalized PL spectra for the $FAPbBr_3@SiO_2$ sample with precursor load/interparticle separation 5%/28nm before (red) and after (black curve) irradiation with CW laser light for 5 minutes.

S.6 Activation/recovery PL curves for samples passivated with PMMA:

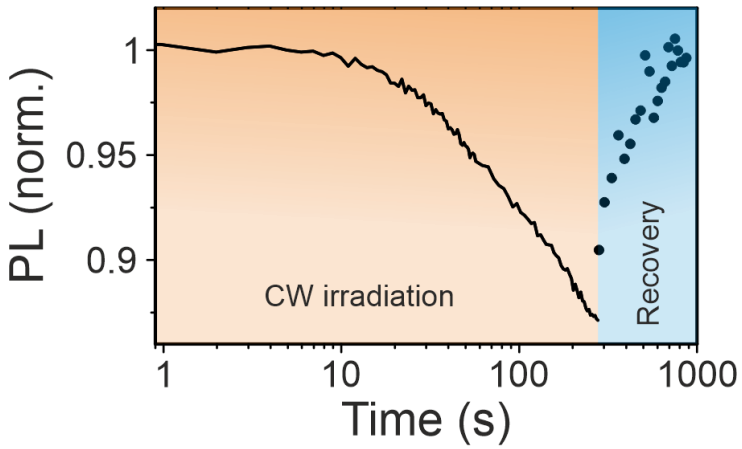

Figure S6: Time evolution of the PL maximum for a $FAPbBr_3@PMMA@SiO_2$ sample with C_{prec}=20% infiltrated with PMMA under CW irradiation (orange box) and during recovery in the dark (blue box).

S.7 Spectral evolution of PL under CW irradiation for passivated samples:

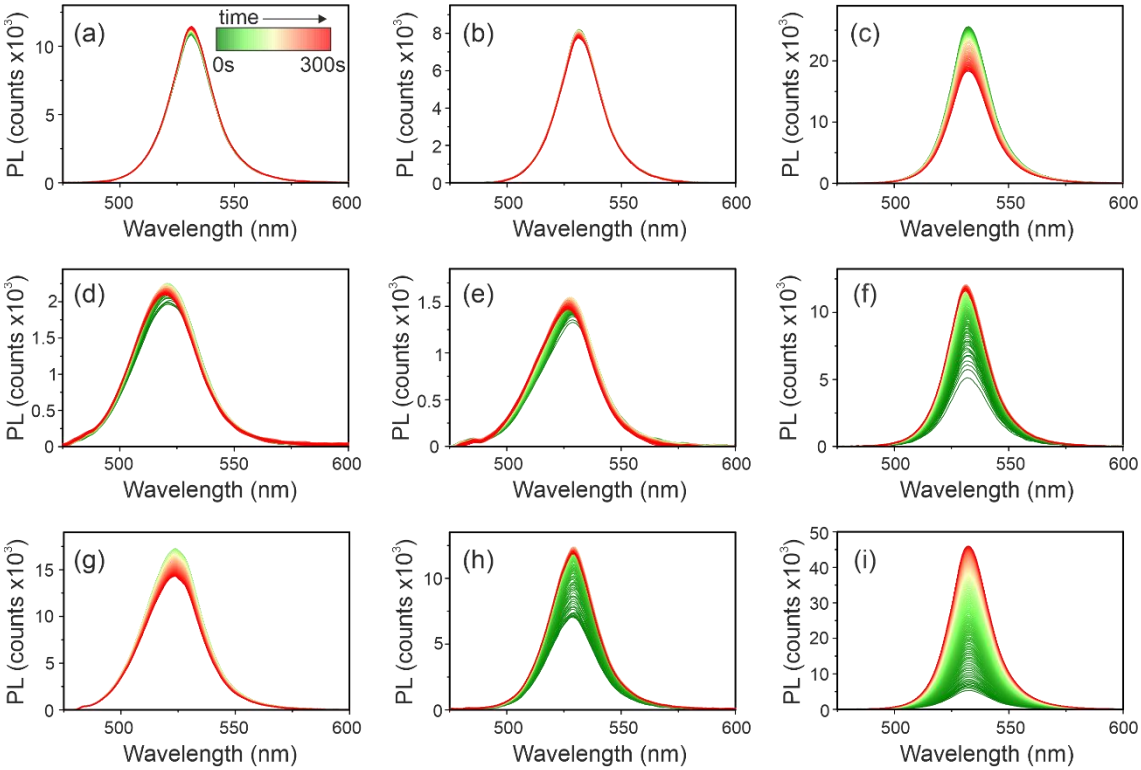

Figure S7: PL spectra collected at different times (same time span as in Figure 1 in the main text) under CW irradiation for samples with different precursor load/average interparticle separation (left (5%/28nm), center (10%/22nm) and right (20%/15nm)) column) with different passivating agents: PMMA (a-c), O_2 (d-f) and humid air (g-i).

S.8 Activation/recovery PL curves for samples exposed to an O_2 atmosphere:

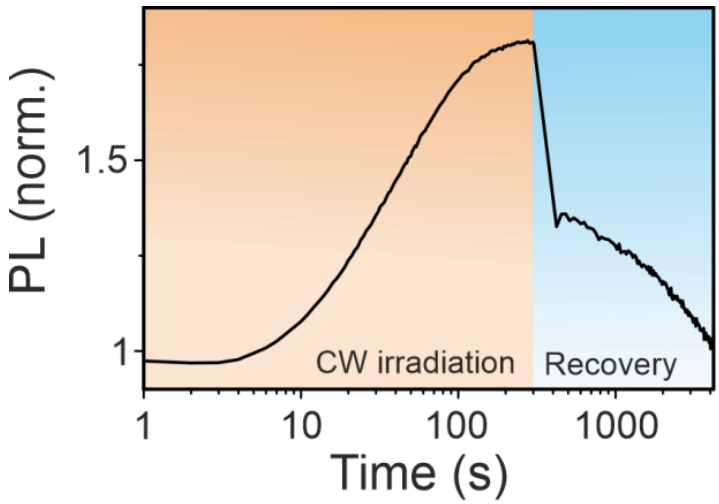

Figure S8: Time evolution of the PL maximum for a sample with C_{prec}=20% exposed to an O_2 atmosphere under CW irradiation (orange box) and during recovery in the dark (blue box).

S.9 Activation/recovery PL curves for samples exposed to a humid air atmosphere:

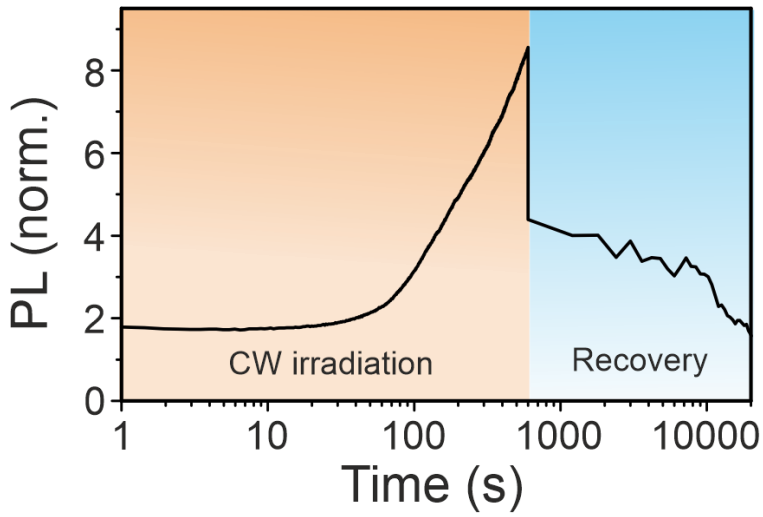

Figure S9: Time evolution of the PL maximum for a sample with C_{prec}=20% exposed to a humid air atmosphere under CW irradiation (orange box) and during recovery in the dark (blue box).

S.10 Lognormal fits of TRPL data for samples fabricated with 5% precursor and exposed to different passivating agents:

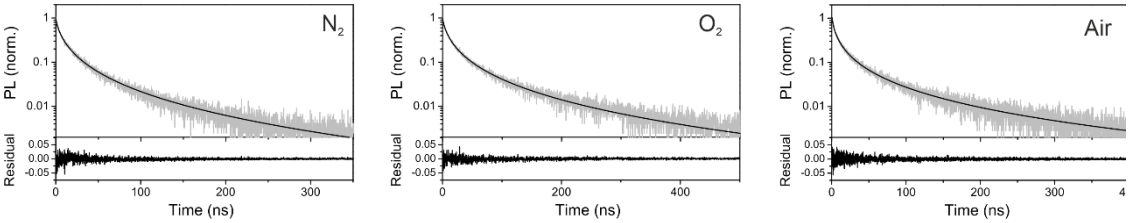

Figure S10: Lognormal fits (black curve) to experimental TRPL data (grey data) and the residual of the fit for three different atmospheres.

---

[1] Tiede, D.O.; Romero-Pérez, C.; Koch, K.A.; Ucer, B.; Calvo, M.E.; Kandada, A.R.K.; Galisteo-López, J.F.; Míguez, H. Effect of Connectivity on the Carrier Transport and Recombination Dynamics of Perovskite Quantum-Dot Networks. *ACS Nano* **2024**, *18*, 2325-2334.